VECTOR MESON PRODUCTION IN DIFFRACTIVE DIS: COLOR DIPOLE PHENOMENOLOGY*

I.P. Ivanov

IFPA, Université de Liège
place du 20-Août 9, 4000 Liège, Belgium
and
Sobolev Institute of Mathematics
4 Acad. Koptyug Ave., 630090 Novosibirsk, Russia

(Received May 12, 2008)

In these lectures, we first review the main steps in the calculation of diffractive vector meson production within the color dipole approach, and then compare the results with experimental data from HERA.

PACS numbers: 13.60.Le

1. What is special about diffractive VM production?

Vector meson production in diffractive DIS, $\gamma^* p \to Vp$, offers a very rich set of dependences to explore in experiment, Fig. 1, left. One can check how the cross-section depends on the total $\gamma^* p$ energy W, on the photon's virtuality Q^2, on the momentum transfer squared t, and also test multiple correlations (for example, one can study how the energy-rise exponent changes with Q^2). All these kinematical parameters can be controlled independently and continuously, allowing one to see in full detail the transition from soft to hard diffraction in a much cleaner fashion than, for example, in the inclusive DIS. One can also compare production cross-section for different mesons, either in the same (*e.g.* ρ, ρ', ρ'', ρ_3) or different (ρ, ω, ϕ, J/ψ, Υ) isospin-flavor states. Finally, by detecting the scattered electron and studying the angular dependence of the decay product of the vector meson, one can reconstruct the helicity structure of the production amplitude in its full complexity.

* Presented at the School on QCD, Low-x Physics, Saturation and Diffraction, Copanello, Calabria, Italy, July 1–14, 2007.

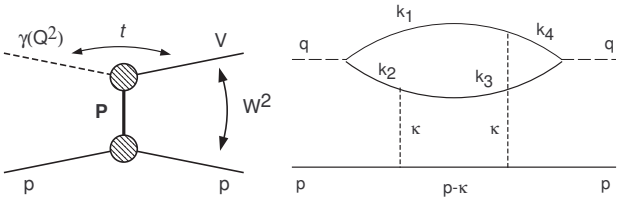

Fig. 1. Left: kinematics of the diffractive VM production via the Pomeron, $\mathbb{P}$, exchange in the t-channel. Right: a typical starting diagram for the calculation of the total photoabsorption cross-section $\sigma_{\rm tot}(\gamma^* p)$.

From theoretical side, diffractive VM production takes place in a unique kinematical regime, where various theoretical approaches can be tested. They range from simple phenomenological Regge-type models for the energy behavior or a vector dominance inspired model for the Q^2-dependence at small virtualities, to full-fledged pQCD and BFKL calculations. One can hope that such a clash of various theoretical ideas will lead to a better understanding of the dynamics of strong interactions.

In these lectures, we will focus only on one particular approach: the color dipole, or $k_{\rm t}$-factorization, approach. We will first underline main steps in the application of this approach to diffractive VM production, and then discuss the experimental data in this language. More details can be found in a recent review [1].

2. Basics of the color dipole approach

Let us start with a classical topic in hadronic physics, the Vector Dominance Model (VDM), see *e.g.* [2]. In the original formulation, the physical photon is represented as a sum of a bare photon and of a "hadronic" part of the photon, $|\gamma^*(Q^2)\rangle = |\gamma^*(Q^2)\rangle_{\rm bare} + |\gamma^*(Q^2)\rangle_{\rm h}$. This hadronic part is represented as an integral over all possible asymptotic (in respect to strong interactions) hadronic states with photon's quantum numbers and with invariant mass M. At not too large masses, the dispersion integral over M is saturated by the lowest resonances. Such contributions can then be *defined* as contributions of vector mesons. For example, in the ρ-meson flavor-isospin sector, one can rewrite the hadronic part of the virtual photon as

$$|\gamma^*\left(Q^2\right)\rangle_{\rm h} = \sum_V \frac{e}{f_V} \frac{m_V^2}{m_V^2 + Q^2} |V\rangle\,, \tag{1}$$

where f_V is the e^+e^- decay constant. With this representation, the amplitude of diffractive production of a vector meson V can be written as

$$\mathcal{A}\left(\gamma^* p \to V p\right) = \sum_{V'} \frac{e}{f_{V'}} \frac{m_{V'}^2}{m_{V'}^2 + Q^2} \left\langle V|\hat{\sigma}|V'\right\rangle \,. \tag{2}$$

Diffraction operator $\hat{\sigma}$ introduced here describes how various states V scatter among each other upon diffractive collision; it incorporates all the microscopic dynamics of diffraction.

At small Q^2 the ground state pole dominates in the dispersion integral. If one assumes that the subsequent scattering process is diagonal in the space of states $|V\rangle$, then (2) gives a closed expression for the amplitude of the production of the ground state meson in a given flavor channel. For example, for the ρ-meson one can write

$$\mathcal{A}(\gamma^* p \to \rho p) \approx \frac{e}{f_\rho} \frac{m_\rho^2}{m_\rho^2 + Q^2} \langle \rho|\hat{\sigma}|\rho\rangle \,. \tag{3}$$

This simple Ansatz gives a reasonable description of the ρ-production cross-section in the small-Q^2 region.

The origin of VDM success becomes transparent in the *color dipole approach*, [3]. It applies to the frame where the projectile momentum is large, so that the transverse motion of its partons is relativistically slowed down. In a high-energy diffractive reaction, the scattering amplitude has form $\mathcal{A}(A \to B) = \langle B|\hat{\sigma}|A\rangle$, where diffractive states are represented as coherent combinations of multipartonic Fock states:

$$|A\rangle = \Psi^A_{q\bar{q}}|q\bar{q}\rangle + \Psi^A_{q\bar{q}g}|q\bar{q}g\rangle + \dots \,, \tag{4}$$

where integration over all internal degrees of freedom is assumed. Since the transverse motion is suppressed by γ-factor, *i.e.* by power of W^2, $\hat{\sigma}$ becomes diagonal in this impact parameter representation. Since the lowest Fock state (color dipole $q\bar{q}$) dominates, the diffraction operator can be expressed via the color dipole cross-section $\sigma_{\rm dip}(\vec{r})$ of a dipole with transverse separation $\vec{r}$. The transition amplitude is represented as

$$\mathcal{A}(A \to B) = \int dz d^2\vec{r}\, \Psi^{B*}_{q\bar{q}}(z,\vec{r}) \sigma_{\rm dip}(\vec{r}) \Psi^A_{q\bar{q}}(z,\vec{r}) \,, \tag{5}$$

where z is the quark's fraction of the lightcone momentum of particle A.

The origin of the VDM success in photoproduction reactions ($A = |\gamma^*\rangle_{\rm h}$) lies in the fact that the typical wave functions of the ground state vector meson used in phenomenology are very similar to the transverse photon lightcone wave function at small Q^2. As virtuality Q^2 grows, the $q\bar{q}$ wave function of the photon shrinks, while the color dipole cross-section behaves as $\sigma_{\rm dip} \propto r^2$ at small r and reaches a plateau at large r. As a result, the

function under integral (5), where $A \equiv \gamma^*$ and B is a ground state vector meson, peaks at the scanning radius $r_S \sim 6/\sqrt{Q^2+M^2}$, [4]. At small Q^2 the typical scanning radius is large, and the amplitude is roughly proportional to the integration measure

$$\mathcal{A}(\gamma^* \to V) \propto r_S^2 \propto \frac{1}{Q^2+M^2}\,,$$

which mimics the VDM behavior. At larger Q^2 the scanning radius becomes small and the diffraction cross-section itself decreases. This phenomenon of color transparency produces a more rapid decrease $A(\gamma^* \to V) \propto 1/(Q^2+M^2)^2$ up to logarithmic factors, [3, 4].

At large Q^2, $\Psi^{\gamma}_{q\bar{q}}(Q^2)$ is a coherent superposition of many $J^{\mathrm{PC}} = 1^{--}$ mesons, including radial and orbital excitations, and transitions $\langle V|\hat{\sigma}|V'\rangle$ must be taken into account. Generalized VDM remains formally correct, but becomes very impractical and misses the insight.

Here, we also note that there is a number of deep theoretical issues related to the color dipole approach. First, it is closely related to the BFKL approach, [5], see review [6]. The latter is usually formulated in the transverse momentum representation, but the important role of the coordinate representation has been known since 1986, [7]. At the leading order, one can enrich BFKL dynamics with running α_S and effective gluon propagation radius to obtain generalized BFKL evolution of dipole cross-section, [8]. At NLO, BFKL kernel was also reformulated in the coordinate representation recently, [9].

Insight into the origin/limitations of the color dipole formalism from non-perturbative treatment of the $\gamma^* p$ scattering is given in [10].

3. $\sigma_{\mathrm{tot}}(\gamma^* p)$ in k_{t}-factorization

To show the main steps in a typical diffractive calculation within the color dipole approach, consider the simplest example: the imaginary part of the forward elastic scattering amplitude $A(\gamma^* p \to \gamma^* p)$, which is related to the total photoabsorption cross-section $\sigma_{\mathrm{tot}}(\gamma^* p)$, via the optical theorem.

The calculations are done mostly easily by direct analysis of the Feynman diagrams in the k_{t}-factorization representation, which is just the Fourier transform of the color dipole approach. We will start with the lowest order pQCD diagrams for photon–quark scattering at high energies and then show how to pass from a quark to the proton by introducing the unintegrated gluon density of the proton.

3.1. Born-level calculation

At high energy, the dominant contribution to the forward elastic $\gamma^* q$ scattering comes from two-loop diagrams such as shown in Fig. 1, right. Its amplitude is

$$A = 4\pi\alpha_{\rm em}\sum_f e_f^2\, C\int\frac{d^4k}{(2\pi)^4}\frac{d^4\kappa}{(2\pi)^4}\frac{\bar u_q\gamma^{\nu'}(\hat p-\hat\kappa)\gamma^{\mu'}u_q}{(p-\kappa)^2+m^2+i\varepsilon}\cdot\frac{g_{\mu\mu'}}{\kappa^2+i\varepsilon}\cdot\frac{g_{\nu\nu'}}{\kappa^2+i\varepsilon}$$
$$\times\frac{{\rm Tr}[(\hat k_1+m)\hat e_{\lambda_i}(\hat k_2+m)\gamma^\mu(\hat k_3+m)\hat e^*_{\lambda_f}(\hat k_4+m)\gamma^\nu]}{\prod(k_i^2-m^2+i\varepsilon)}\,. \tag{6}$$

Here k and κ are momenta inside the quark and gluon loops, respectively, e_f is the electric charge of the quark of flavor f, C is the color factor. At high energies, this two-loop amplitude can be simplified with the help of the Sudakov decomposition of the particles' momenta. Let us introduce two lightcone vectors p'^μ and q'^μ, $s\equiv(p'+q')^2=2p'q'$, such that

$$q^\mu=q'^\mu+\frac{Q^2}{s}p'^\mu\,,\qquad p^\mu=p'^\mu+\frac{m^2}{s}q'^\mu\,,$$

and decompose integration momenta as $k^\mu=zq'^\mu+yp'^\mu+\vec k^\mu$ and $\kappa^\mu=\beta q'^\mu+\alpha p'^\mu+\vec\kappa^\mu$, where arrows indicate vectors with transverse components only. Then, integration, for example, over d^4k becomes $s\,dy\,dz\,d^2\vec k/2$. It turns out that among four integrals over Sudakov's variables $dy\,dz\,d\alpha\,d\beta$ two can be immediately calculated via residues. After some algebra (see details in [11]) one rewrites the imaginary part of the longitudinal integral as

$${\rm Im}\int\frac{dy\,dz\,d\alpha d\beta}{\text{propagators}}=\frac{4\pi^2}{s^3}\int\limits_0^1\frac{dz}{z^2(1-z)^2}\frac{1}{(Q^2+M^2)^2}\frac{1}{(\vec\kappa^2)^2}\,, \tag{7}$$

where $M^2=(\vec k^2+m^2)/z(1-z)$ is the invariant mass of the $q\bar q$ pair.

The next step is to "decouple" the Lorentz indices of the upper quark loop and the lower line. This can be done by rewriting

$$g_{\mu\mu'}=\frac{2}{s}q'_\mu p'_{\mu'}+\frac{2}{s}p'_\mu q'_{\mu'}+g^\perp_{\mu\mu'}\,,$$

and checking that at large s the first term dominates. The lower line then becomes $\bar u_q\hat q'(\hat p-\hat\kappa)\hat q' u_q\approx s^2\delta_{\zeta\zeta'}$, while the trace over the quark loop is

$${\rm Tr}\left[\left(\hat k_1+m\right)\hat e_{\lambda_i}\left(\hat k_2+m\right)\hat p'\left(\hat k_3+m\right)\hat e^*_{\lambda_f}\left(\hat k_4+m\right)\hat p'\right]\,.$$

Although this trace can be calculated explicitly, there is a more efficient approach based on the lightcone spinors. We first note that among the four quark lines, two (k_1 and k_3) are already on-mass-shell because of the residues. The other two can be also put on mass shell by the following trick

$$\hat{k}_2 + m = \hat{k}_2^{\text{on-shell}} + m + \frac{k^2 - m^2}{s}\hat{p}' \to \hat{k}_2^{\text{on-shell}} + m\,,$$

since $\hat{p}'\hat{p}' = p'^2 = 0$. Thus, in the trace all spinors can be treated on-mass-shell. One can then replace $\hat{k} + m \to \sum_\zeta u\bar{u}$ for quarks and $-\sum_\zeta v\bar{v}$ for antiquarks, and represent the trace as a product of scalar building blocks describing $\gamma \to q\bar{q}$ or $qg \to q$ vertices.

Repeating this calculation for the other diagrams (with two gluons coupled to the $q\bar{q}$ pair in different ways), one gets for the longitudinal (L) and transverse (T) photon:

$$\text{Im}A_{\text{L/T}} = s\frac{8\alpha_{\text{em}}\sum_f e_f^2}{3\pi^2}\int dz\; d^2k \frac{d^2\kappa}{\kappa^4}\alpha_{\text{S}}^2 W_{\text{L/T}}\,, \tag{8}$$

with

$$W_{\text{T}} = m^2\Phi_2\Psi_2 + \left[z^2 + (1-z)^2\right]\vec{\Phi}_1\vec{\Psi}_1\,, \qquad W_{\text{L}} = 4z^2(1-z)^2Q^2\Phi_2\Psi_2\,. \tag{9}$$

Here $\Psi_2 = 1/[z(1-z)(M^2+Q^2)]$ and $\vec{\Psi}_1 = \vec{k}\Psi_2$, while Φ_2 and $\vec{\Phi}_1$ are the coherent sums of initial photon's wave functions over four diagrams: $\Phi_2 = \sum(-1)^a\Psi_2(z,\vec{k}_a)$, $\vec{\Phi}_1 = \sum(-1)^a\vec{\Psi}_1(z,\vec{k}_a)$.

3.2. Unintegrated gluon density

In the famous equivalent photon approximation [12] for the electron scattering off a target, one writes the cross-section as a product of photon-target cross-section multiplied with the differential density of equivalent photons inside an electron with given transverse momentum $\vec{\kappa}$ and fraction of electron lightcone momentum x_γ. At small x_γ one has

$$\mathcal{F}(x_\gamma,\vec{\kappa}^2) \equiv \frac{dn_e^\gamma}{d\log x_\gamma d\log\vec{\kappa}^2} = \frac{\alpha_{\text{em}}}{\pi}\left(\frac{\vec{\kappa}^2}{\vec{\kappa}^2+\kappa_z^2}\right)^2\,. \tag{10}$$

A similar density of equivalent photons can be defined also for a neutral system made of charged particles. For example, in positronium one has

$$\mathcal{F}(x_\gamma,\vec{\kappa}^2) = \frac{\alpha_{\text{em}}}{\pi}\left(\frac{\vec{\kappa}^2}{\vec{\kappa}^2+\kappa_z^2}\right)^2 N\,\left[1 - F_2\left(\vec{\kappa}^2\right)\right]\,,$$

where $F_2(\vec{\kappa}^2)$ is two-particle formfactor and $N = 2$ is the number of constituents in positronium.

Similar considerations apply for the unintegrated gluon density in proton, [13]. One can represent the cross-section of the $\gamma^* q$ scattering as the flux of gluons in the quark multiplied by the $\gamma^* g$ cross-section. Then, switching from a single quark to the proton, on can define the Born-level unintegrated density of gluons in the proton:

$$\mathcal{F}_g^{\rm Born} = C_F N_c \frac{\alpha_{\rm s}}{\pi} \left[1 - F_2\left(\vec{\kappa}^2\right)\right] .$$

In contrast to the equivalent photons, the t-channel gluons interact, and their interaction modifies the unintegrated gluon density: $\mathcal{F}_g^{\rm Born} \to \mathcal{F}_g(x_g, \vec{\kappa}^2)$. We do not calculate $\mathcal{F}_g(x_g, \vec{\kappa}^2)$, but just assume that it is a well-defined quantity independent of the upper subprocess. This is the main assumption behind the $k_{\rm t}$-factorization approach.

With this prescription, the final expression for the total photoabsorption cross-section is

$$\sigma_{\rm L/T} = \frac{\alpha_{\rm em} \sum e_f^2}{\pi} \int dz\; d^2k \frac{d^2\kappa}{\kappa^4} \alpha_{\rm S} \mathcal{F}(x_g, \vec{\kappa}^2) W_{\rm L/T} ,$$

The corresponding structure functions are:

$$F_{\rm L/T} = \frac{Q^2}{4\pi^2 \alpha_{\rm em}} \sigma_{\rm L/T} , \qquad F_2 = F_{\rm L} + F_{\rm T} .$$

Now, it is also instructive to see the result in the transverse coordinate (impact parameter) representation. To the leading $\log(1/x)$, the quark loop momentum $\vec{k}$ enters the amplitude only via the initial and final photon wave function, Ψ_i and Φ_i, respectively. After 2D Fourier transformation this leads to $\vec{r}_i = \vec{r}_f$, *i.e.* the color dipole remains frozen in the transverse space. The photoabsorption cross-section takes form

$$\sigma_{\rm L/T} = \int\limits_0^1 dz \int d^2\vec{r}\, \left|\Psi_{\rm L,T}(z, \vec{r})\right|^2 \sigma_{\rm dip}(\vec{r}) , \tag{11}$$

where the photon lightcone WFs come form the Fourier transform of Ψ_i and Φ_i, while the dipole cross-section is defined as

$$\sigma_{\rm dip}(\vec{r}) = \frac{4\pi}{3} \int \frac{d^2\vec{\kappa}}{\kappa^4} \alpha_{\rm s} \mathcal{F}(x_g, \vec{\kappa}^2) \left[1 - \cos(\vec{\kappa}\vec{r})\right] . \tag{12}$$

Thus, not only have we proved expression (5) in the particular case of the forward photon scattering, but also found the expression for the color dipole cross-section and the lightcone WF of the photon. Later, when calculating VM production, we will assume that the incoming photon is described by the same WF, and the the color dipole cross-section (or unintegrated gluon density) is given by the same expression, corrected for the off-forward kinematics.

3.3. Properties of $\sigma_{\rm dip}(r)$ *and* $\mathcal{F}(x_g, \vec{\kappa}^2)$

Having expressed the photoabsorption cross-section in terms of unintegrated gluon density or the color dipole cross-section, one can now use the experimental data on structure function F_{2p} to get insight into the shape and properties of these two quantities.

This analysis has been conducted independently by several groups, which resulted in various parametrizations of $\sigma_{\rm dip}(r)$ and $\mathcal{F}(x_g, \vec{\kappa}^2)$. Here, we describe salient features of these results.

At small dipole sizes, $r \ll 1$ fm, the color dipole cross-section is small, $\sigma_{\rm dip}(\vec{r}) \propto r^2$ up to logarithmic corrections, see Eq. (12). This is a manifestation of the famous color transparency, [3]. In this region, one can safely talk about exchange of perturbative gluons. For large dipoles, $r \gtrsim 1$ fm, the color dipole cross-section reaches a plateau at some tens of millibarns, which is often viewed as one of the sides of the saturation. Typical dipoles sizes where the transition takes place gradually shift towards smaller r as the energy increases. In the first approximation, one can also assume that this shift occurs without changing the shape of $\sigma_{\rm dip}(r)$. This idea leads to interesting consequences, for example, to the so-called geometric scaling in inclusive photoabsorption, [14], and in VM production [15]. The color dipole cross-section as non-zero transverse momentum transfer was studied in [16].

A very illustrative example is the famous Golec-Biernat–Wüsthoff saturation model for $\sigma_{\rm dip}(r)$, [17]:

$$\sigma_{\rm dip}(r) = \sigma_0 \left[1 - \exp\left(-r^2 Q_{\rm s}^2(x)\right)\right] , \tag{13}$$

where $\sigma_0 = 23$ mb, $Q_{\rm s}^2(x) = 0.0238\ \text{GeV}^2\, x^{-0.29}$ is saturation scale. Despite being rather simple, this model incorporates the above mentioned features and gives a fair description of the F_{2p}. Its further improvement can be found in [18].

The unintegrated gluons density $\mathcal{F}(x_g, \vec{\kappa}^2)$ can also be extracted from the $F_2(x, Q^2)$ data. Its main features are: at fixed x_g and large gluon momenta it approaches the pQCD prediction based on differentiating the conventional gluon densities: $\mathcal{F}_{pt}(x_g, \vec{\kappa}^2) \equiv \partial G(x_g, \vec{\kappa})/\partial \log \vec{\kappa}^2$. However, $\mathcal{F}_{pt}(x_g, \vec{\kappa}^2)$ is insufficient for the description of processes at small-to-moderate momenta,

where one must add an intrinsically soft part. At extremely small momenta, when the gluon's wavelength is larger than the proton, $\mathcal{F}(x_g, \vec{\kappa}^2)$ should decreases due to color-neutrality of the proton. Examples of such fits can be found in [13, 19].

An important check of the universality of the fits obtained is that they reproduce well the charm quark contribution to $F_2(x, Q^2)$ and the longitudinal structure function, $F_{\rm L}(x, Q^2)$, [20].

The color dipole cross-section and the unintegrated gluon density represent the same physical quantity, just viewed from different angles. Both languages are useful in different contexts. For scattering of small dipoles large $\vec{\kappa}^2$ dominate, and the process can be convenient described in terms of $\mathcal{F}(x_g, \vec{\kappa}^2)$. At large dipoles, where the soft exchange dominates and there are almost no perturbative gluons, discussion in terms of color dipole cross-section is more natural. Formally, one can still present cross-sections involving unintegrated gluon density, but in this region it just stands for "Fourier transform of $\sigma_{\rm dip}$".

4. Exclusive diffractive production of vector mesons

The forward $\gamma^* p$ scattering amplitude can be extended analytically to the non-diagonal transition: $\gamma^*(Q_1^2)p \to \gamma^*(Q_2^2)p$ (DVCS would correspond to $Q_2^2 = 0$). If virtualities remain much smaller than W^2, all the essential detail of the calculation remain the same, and the amplitude can be presented analogously to (8):

$$\mathrm{Im}A(Q_1^2, Q_2^2) \propto \int dz d^2\vec{k} \frac{d^2\vec{\kappa}}{(\vec{\kappa}^2)^2} \mathcal{F}(x_1, x_2, \vec{\kappa}^2) W(Q_1^2, Q_2^2)\,. \qquad (14)$$

Expressions $W(Q_1^2, Q_2^2)$ are calculable as before, while the unintegrated gluon distribution becomes skewed $\mathcal{F}(x_1, x_2, \vec{\kappa}^2)$, since $x_1 \neq x_2$. Amplitude (14) can be even extended to the timelike region, $Q_2 = -m_V^2$. So, in order to pass to the VM production, one needs to replace the final photon LC WF with vector meson LC WF, $\Psi_V(z, \vec{k})$, and take into account the fact that $q\bar{q}$ pair can represent different mesons (ground state, excited, high-spin).

To understand the spin-orbital structure of the $q\bar{q}V$ coupling, recall first the nonrelativistic example of the proton–neutron–deuteron coupling:

$$\phi_n^\dagger \left[\sigma^i u(\boldsymbol{p}) + D^{ij}\sigma^j w(\boldsymbol{p})\right] \phi_p \cdot V^i$$

Here V^i is polarization vector; $u(\boldsymbol{p})$ and $w(\boldsymbol{p})$ are spherically symmetric radial WFs; σ^i is spinorial structure for the S-wave component, while $D^{ij} = 3\boldsymbol{p}^i\boldsymbol{p}^j - \delta^{ij}\boldsymbol{p}^2$ produces the D-wave spinorial structure.

A similar approach is to be used when constructing the $q\bar{q}V$ coupling: $\bar{u}'\Gamma^\mu u \cdot V_\mu \cdot \Psi_V(\boldsymbol{p})$. Here spinorial structures Γ^μ (which do not coincide with γ^μ!) are to be constructed for S-wave and D-wave VM, while the radial wave function $\Psi_V(\boldsymbol{p})$ is spherically symmetric (in VM rest frame) and is independent of the polarization state (no Ψ_T, no Ψ_L, just $\Psi(\boldsymbol{p}^2)$). Here, 3D-vector $\boldsymbol{p}$ is the half of the relative momentum in the $q\bar{q}$ pair in the pair rest frame; in the lab frame $\boldsymbol{p}^{\,2} = \vec{p}^2 + p_z^2$, where $\vec{p} = \vec{k}$, $p_z = (2z-1)M/2$.

The spinorial structure Γ^μ_S for the S-wave state can be constructed via Melosh transform or simply by requiring that the function in the normalization integral depends only on $\boldsymbol{p}^2$:

$$\Gamma^\mu_\mathrm{S} = \gamma^\mu + \frac{2p^\mu}{M+2m}\,.$$

It differs from naive γ^μ vertex by Fermi motion correction, which is important not only for light VM, but also for J/ψ. The D-wave structure is obtained by contracting Γ^μ_S with the D-wave tensor, [21]:

$$\Gamma^\mu_D = D^{\mu\nu}\Gamma^\nu_\mathrm{S} = \gamma^\mu + \frac{M+m}{\boldsymbol{p}^2}p^\mu\,.$$

The resulting expression for the amplitudes

$$\begin{aligned}\frac{1}{s}\mathrm{Im}A(\lambda_V,\lambda_\gamma) \;=\; & \frac{c_V\sqrt{4\pi\alpha_\mathrm{em}}}{4\pi^2}\int\frac{dzd^2\vec{k}}{z(1-z)}\frac{d^2\vec{\kappa}}{(\vec{\kappa}+\vec{\Delta}/2)^2(\vec{\kappa}-\vec{\Delta}/2)^2}\\ & \times\alpha_\mathrm{s}\mathcal{F}(x_1,x_2,\vec{\kappa},\vec{\Delta})\cdot W^{S/D}(\lambda_V,\lambda_\gamma)\,. \qquad (15)\end{aligned}$$

c_V is flavor-averaged charge: $c_v = 1/\sqrt{2}$, $1/3\sqrt{2}$, $-1/3$, $2/3$ for $\rho,\omega,\phi,J/\psi$. The list of $W^{S/D}(\lambda_V,\lambda_\gamma)$ can be found in [11, 21]. Using Eq. (15), one can calculate diffractive production of any VM.

5. Understanding experimental data with the color dipole approach

Since the Pomeron has vacuum quantum numbers, diffractively produced mesons must have $P = C = -1$. Other quantum numbers are not fixed: the mesons can be either ground states ($\rho,\omega,\phi,J/\psi,\Upsilon$), or radially, orbitally or spin-excited states. In the ρ system, these are often identified with $\rho'(1450)$, $\rho''(1700)$, $\rho_3(1690)$, respectively. Most of the data accumulated and theoretical calculations performed so far concern the ground states, so this will be the main focus.

5.1. Q^2 dependence

In theory, the main Q^2-dependence of the VM production cross-section can be read off from the color dipole expression

$$\frac{1}{s}\mathrm{Im}\mathcal{A}(Q^2) = \int dz\ d^2\vec{r}\ \Psi_V^*(z,\vec{r})\sigma_{\mathrm{dip}}(\vec{r})\Psi_\gamma(z,\vec{r})\,. \tag{16}$$

The photon LCWF shrinks as Q^2 grows: $\Psi_\gamma \sim \exp(-\overline{Q}r)$, where $\overline{Q}^2 = z(1-z)Q^2 + m^2$. With the properties of the color dipole cross-section, the transverse integral in (16) comes roughly from r close to the so-called scanning radius, [4], $r_{\mathrm{S}} \approx 6/\sqrt{Q^2+m_V^2}$, which allows one to study soft-hard transition in diffraction in a controllable manner.

The amplitude of small Q^2 production of light VM is saturated by the integration measure, $A_{\mathrm{T}}(Q^2) \propto r_{\mathrm{S}}^2 \propto 1/(Q^2+m_V^2)$, which mimics the vector dominance model result. At large $Q^2 + M_V^2$ color transparency comes into play, $A(Q^2) \propto r_{\mathrm{S}}^2\sigma_{\mathrm{dip}}(r_{\mathrm{S}}^2)$, which leads to a steeper Q^2-dependence:

$$d\sigma_{\mathrm{L}} \propto Q^2\frac{\left[\alpha_{\mathrm{S}}G\left(x,\overline{Q}^2\right)\right]^2}{\left(Q^2+m_V^2\right)^4}\,, \qquad d\sigma_{\mathrm{T}} \propto \frac{\left[\alpha_{\mathrm{S}}G\left(x,\overline{Q}^2\right)\right]^2}{\left(Q^2+m_V^2\right)^4}\,.$$

Since this cross-section is quadratic in the gluon density, one can hope that diffractive VM production might provide a better means to discriminate among the models of the gluon density than the inclusive DIS. Let us now see what the recent data say.

ρ **production**. Comparison between the experimental data on the Q^2-dependence of the ρ-production and several theoretical calculations is shown in Fig. 2, left. Except for the $Q^2 \sim 1$ GeV^2 region, where the soft-to-hard transition takes place, the shape is well reproduced by theory, however there is large uncertainty in the overall normalization. This is not surprising due to the uncertainties in the description of the ρ-meson VM in the theoretical calculations. Currently, new larger data sets are being analyzed by both ZEUS and H1, [22].

If one wants to extract the gluon densities from these data, one must deal with several complicating issues. First, other factors such as the diffractive slope b and the balance between σ_{L} and σ_{T} depend on Q^2; although this can be eliminated by separately studying $d\sigma_{\mathrm{L}}/dt$ and $d\sigma_{\mathrm{T}}/dt$. Second, the exact knowledge is lacking of the hard scale $\overline{Q}^2$ at which the gluon density is probed. While for heavy quarkonia such as Υ, $\overline{Q}^2 \approx (Q^2+m_V^2)/4$ is probably a good estimate, for light VM the quark Fermi motion makes the scale softer, $\overline{Q}^2 \approx 0.1(Q^2+m_V^2)$. Moreover, these scales for the longitudinal and transverse cross-sections $\overline{Q}_{\mathrm{L}}^2$ and $\overline{Q}_{\mathrm{T}}^2$ are expected to be somewhat

different, [23]. Finally, one can question the applicability of the pQCD approach at all, noting that in the ρ-production even $\overline{Q}^2 = 2$ GeV^2 requires already to $Q^2 \sim 20$ GeV^2. So, it appears that majority of experimental data on ρ production are in the domain where pQCD is not safely applicable. As another indication of this, NLO corrections to the VM production cross-section within the collinear factorization approach [24] were recently found to be huge.

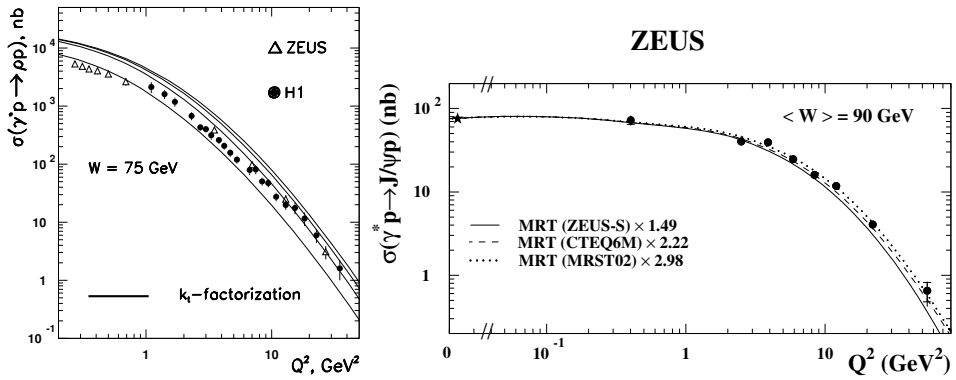

Fig. 2. Comparison between the data and theoretical calculations of the Q^2-dependence of the ρ (left) and J/ψ production cross-sections.

J/ψ **production** was suggested to be a better probe of gluon density, as it contains $m_{J/\psi}$, which might improve the pQCD applicability and stability. An example of the comparison of the ZEUS data with some of the theoretical calculations is shown in Fig. 2, right. One sees that many theoretical calculations, including the ones with different fits for the gluon density, describe well the Q^2-dependence, but are off by a factor of $\lesssim 2$ in the overall normalization. So, diffractive J/ψ-production does not appear to be a particularly good means of distinguishing among the models.

Longitudinal-to-transverse ratio is defined as

$$R = \frac{\sigma_{\rm L}}{\sigma_{\rm T}}\,, \qquad R_{\rm LT} = \frac{\sigma_{\rm L}}{\sigma_{\rm T}}\,\frac{m_V^2}{Q^2}\,.$$

The latter quantity is more convenient as it eliminates some trivial Q^2 dependence due to gauge invariance. The asymptotic value of $R_{\rm LT}$ in the limit of heavy quarkonia with no Fermi motion is one, but in fact even J/ψ is very far from this asymptotic regime. Note that large Q^2 does not fulfill this requirement, *i.e.* theory does *not* predict that $R_{\rm LT} \to 1$ for ρ-production at large Q^2.

Theoretical predictions for this ratio are very sensitive to the details of the VM wave function, so it appears as one of the most model-dependent quantities in this process. Models can describe almost any Q^2-behavior of $\sigma_{\rm L}/\sigma_{\rm T}$; Fig. 3 illustrates this point. So, what theory really predicts for R remains unclear.

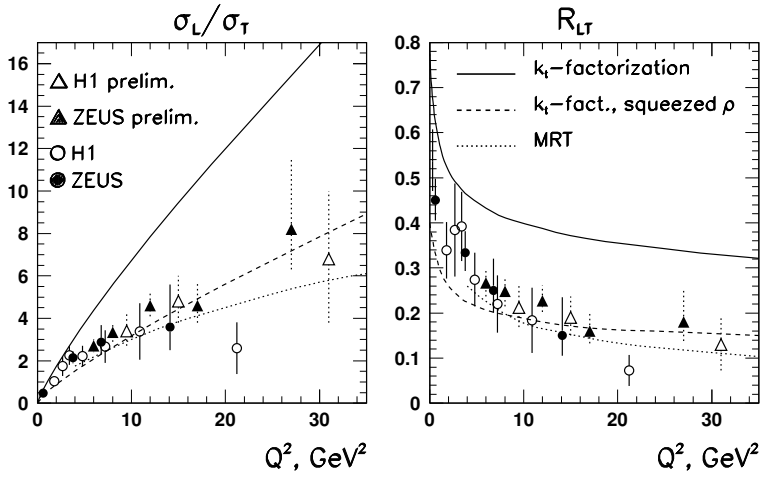

Fig. 3. Longitudinal-to-transverse ratios R (right) and $R_{\rm LT}$ (left) for the ρ-production as functions of Q^2. Solid and dashed lines are the $k_{\rm T}$-factorization calculations with different assumptions for the VM wave-function; dotted line is a prediction from [25] based on the Bloom–Gilman duality arguments.

5.2. Flavor universality: facts and myths

Many parts of the production amplitude depend on Q^2 and m_V^2 through the same scaling quantity $\overline{Q}^2 \approx (Q^2 + m_V^2)/4$. If one compares production cross-section of different mesons at equal $\overline{Q}^2$, then the pQCD estimate is:

$$\frac{1}{\eta_V^{J/\Psi}} \equiv \frac{\sigma(V)}{\sigma(J/\psi)} \approx \frac{m_V \Gamma(V \to e^+e^-)}{m_{J/\Psi}\Gamma(J/\Psi \to e^+e^-)}\,,$$

with $\rho : \omega : \phi : J/\psi = 0.32 : 0.029 : 0.077 : 1$. Therefore, $\eta_V^{J/\Psi}\sigma(V)$ plotted *versus* $Q^2 + m_V^2$ should follow the same trend, which is indeed confirmed by the data.

It is often stated (on the basis of quark charge counting) that theory predicts SU(4) universality in VM production cross-sections: $\rho : \omega : \phi : J/\psi = 1 : 1/9 : 2/9 : 8/9$. We stress that there is no sound theoretical argument for SU(4) universality even at large Q^2, since there are additional flavor-dependent factors (*e.g.* VM wave functions) in the amplitude.

5.3. W-dependence

Since the VM production is a typical diffractive process, the energy dependence of its cross-section is driven by the Pomeron. By changing the hard scale in the VM production, one can hope to see how the properties of the QCD Pomeron depend on this hard scale.

The standard practice to quantify the energy dependence of the VM production cross-section is to fit it by a power law:

$$\sigma(W) \propto W^{\delta}\,, \qquad \delta = 4[\alpha_{\mathbb{P}}(\langle t\rangle) - 1]\,. \tag{17}$$

Here, $\alpha_{\mathbb{P}}(t) \approx \alpha_{\mathbb{P}}(0) + \alpha'_{\mathbb{P}} \cdot t$ is the effective Pomeron trajectory and $\langle t\rangle \approx 1/B$ is the average value of the momentum transfer squared. In the photoproduction limit, there is a robust theoretical prediction

$$\delta_{\Upsilon} > \delta_{\psi(2S)} > \delta_{J/\psi} > \delta_{\phi} > \delta_{\rho}\,,$$

which is indeed confirmed experimentally. As Q^2 increases, the process becomes harder, and $\delta = \delta(Q^2)$ also rises, both in theory and in experiment. If plotted against the scaling variable $Q^2 + m_V^2$, δ for different vector mesons again becomes a universal function.

Although the parametrization (17) is inspired by the Regge theory, one must take extreme care when interpreting the data in this language. For example, one must understand that whenever effective intercept depends on Q^2, the Regge factorization is broken. A nice illustration of this point is given by the ratio of diffractive VM to total inclusive cross-sections:

$$r_{\mathrm{tot}}^{V} = \frac{\sigma_{\gamma^* p \to Vp}\left(W^2, Q^2\right)}{\sigma_{\mathrm{tot}}^{\gamma^* p}\left(W^2, \overline{Q}^2\right)}\,,$$

where $\overline{Q}^2 = (Q^2 + m_V^2)/4$ is chosen in such a way that makes the hard scales of the two processes approximately equal. Naively, one might think that since VM production cross-section is quadratic in the Pomeron exchange, while the total inclusive cross-section is linear, this ratio should exhibit a noticeable W-rise. However, experiment shows [26] that this ratio is roughly constant for ρ meson at all Q^2, but it strongly rises for J/ψ.

However, since the Pomeron is not an isolated Regge pole with fixed $\alpha_{\mathbb{P}}$, the effective energy rise exponents for $\sigma(\gamma^* p \to Vp) \propto [G(x, \overline{Q}^2)]^2$ and $\sigma_{\mathrm{tot}}(\gamma^* p) \propto \int d \log \overline{Q}^2 G(x, \overline{Q}^2)$ are different. Detailed k_{t}-factorization calculations indeed confirm experimental findings, [1].

5.4. Helicity structure

Both the virtual photon and the final vector meson can have three polarization states, leading to five independent helicity amplitudes $A(\lambda_V;\lambda_\gamma)$: helicity-conserving ($A_{11}$, A_{00}) and helicity-violating ones (A_{01}, A_{10}, A_{1-1}). For the strictly forward production, exact s-channel helicity conservation (SCHC) takes place: $\lambda_V = \lambda_\gamma$. However, at non-zero transverse momentum transfer $\vec{\Delta}$, $A(\lambda_V;\lambda_\gamma) \propto |\vec{\Delta}|^{|\lambda_V-\lambda_\gamma|}$. Since the cross-section is concentrated inside the diffractive cone, $d\sigma/dt \propto \exp(-B|t|)$, with $B \approx 4-10$ GeV^{-2}, typical $|\vec{\Delta}|$ is small, which makes the contribution of the helicity violating transitions also small. Hierarchy among helicity amplitudes can be established, [27].

Experimentally, one measures the angular distribution of decay products ($\pi^+\pi^-$, *etc.*) and extracts the spin-density matrix elements $r^a_{\lambda\lambda'}$, which can be expressed in terms of helicity amplitudes, [28]. Spin-density matrix for ρ meson has been studied experimentally in much detail, [29]. Experiments confirm SCHC dominance and also reliably observe small violation of SCHC observed, most notably in $r^5_{00} \propto A_{01}$.

5.5. Production of excited mesons

After a decade of data taking at the HERA collider, we have greatly improved our understanding of diffractive production of various *ground state* vector mesons. However, diffractive production of excited states remains relatively unexplored. The only meson that has been studied in some detail is $\psi(2S)$, [30]. For the ρ system, where the radial $\approx \rho(1450)$, orbital $\approx \rho(1700)$, and spin $\rho_3(1690)$ excitations are known, the only publications so far are from old fixed target experiments, *e.g.* Omega experiment at CERN, [31].

Meanwhile, diffractive production of excited ρ-mesons was studied by theorists. There are calculations of such processes based on Bloom–Gilman duality, [32], taking into account only radial WF effects, [33], and based on full k_t-factorization calculations, [34, 35]. Results of these calculations significantly differ in details, but they agree on one point: production of excited states is remarkably different from the ground state mesons. For orbital and spin excitations, the most salient difference is a distinct pattern of helicity amplitudes and the σ_L/σ_T ratio. There is even a prediction [35] that ρ_3 photoproduction should be dominated by helicity violating amplitudes, a situation that has never been seen in diffraction.

Experimental investigation of excited mesons in diffraction is definitely worth pursuing and might tell us new things about diffraction, many of which are not accessible in the ground state VM production.

REFERENCES

[1] I.P. Ivanov, N.N. Nikolaev, A.A. Savin, *Phys. Part. Nucl.* **37**, 1 (2006).

[2] T.H. Bauer, R.D. Spital, D.R. Yennie, F.M. Pipkin, *Rev. Mod. Phys.* **50**, 261 (1978); Erratum *Rev. Mod. Phys.* **51**, 407 (1979).

[3] N.N. Nikolaev, B.G. Zakharov, *Z. Phys.* **C49**, 607 (1991); A.H. Mueller, *Nucl. Phys.* **B335**, 115 (1990); N.N. Nikolaev, *Comments Nucl. Part. Phys.* **21**, 41 (1992).

[4] B.Z. Kopeliovich, J. Nemchik, N.N. Nikolaev, B.G. Zakharov, *Phys. Lett.* **B309**, 179 (1993); J. Nemchik, N.N. Nikolaev, B.G. Zakharov, *Phys. Lett.* **B341**, 228 (1994).

[5] V.S. Fadin, E.A. Kuraev, L.N. Lipatov, *Phys. Lett.* **B60**, 50 (1975); *Sov. Phys. JETP* **45**, 199 (1977); I.I. Balitsky, L.N. Lipatov, *Sov. J. Nucl. Phys* **28**, 822 (1978).

[6] L.N. Lipatov, *Phys. Rept.* **286**, 131 (1997).

[7] L.N. Lipatov, *Sov. Phys. JETP* **63**, 904 (1986) [*Zh. Eksp. Teor. Fiz.* **90**, 1536 (1986)].

[8] N.N. Nikolaev, B.G. Zakharov, V. Zoller, *JETP Lett.* **59**, 6 (1994); *Phys. Lett.* **B328**, 486 (1994).

[9] V.S. Fadin, R. Fiore, A. Papa, *Nucl. Phys.* **B769**, 108 (2006); *Phys. Lett.* **B647**, 179 (2006); V.S. Fadin, R. Fiore, A.V. Grabovsky, A. Papa, *Nucl. Phys.* **B784**, 49 (2007).

[10] C. Ewerz, O. Nachtmann, *Annals Phys.* **322**, 1635 (2007); *Annals Phys.* **322**, 1670 (2007).

[11] I.P. Ivanov, PhD thesis, Bonn University, 2002, `arXiv:hep-ph/0303053`.

[12] V.M. Budnev, I.F. Ginzburg, G.V. Meledin, V.G. Serbo, *Phys. Rept.* **15**, 181 (1974).

[13] I.P. Ivanov, N.N. Nikolaev, *Phys. Rev.* **D65**, 054004 (2002).

[14] A.M. Stasto, K.J. Golec-Biernat, J. Kwiecinski, *Phys. Rev. Lett.* **86**, 596 (2001).

[15] C. Marquet, R. Peschanski, G. Soyez, *Phys. Rev.* **D76**, 034011 (2007).

[16] J. Bartels, K.J. Golec-Biernat, K. Peters, *Acta Phys. Pol. B* **34**, 3051 (2003).

[17] K. Golec-Biernat, M. Wusthoff, *Phys. Rev.* **D59**, 014017 (1999).

[18] J. Bartels, K.J. Golec-Biernat, H. Kowalski, *Phys. Rev.* **D66**, 014001 (2002); E. Iancu, K. Itakura, S. Munier, *Phys. Lett.* **B590**, 199 (2004).

[19] M.A. Kimber, J. Kwiecinski, A.D. Martin, A.M. Stasto, *Phys. Rev.* **D62**, 094006 (2000); A. Szczurek, N.N. Nikolaev, W. Schafer, J. Speth, *Phys. Lett.* **B500**, 254 (2001); A.V. Kotikov, A.V. Lipatov, G. Parente, N.P. Zotov, *Eur. Phys. J.* **C26**, 51 (2002).

[20] H. Jung, A.V. Kotikov, A.V. Lipatov, N.P. Zotov, `arXiv:0706.3793[hep-ph]`.

[21] I.P. Ivanov, N.N. Nikolaev, *JETP Lett.* **69**, 294 (1999).

[22] S. Chekanov *et al.* [ZEUS Collaboration], *PMC Phys.* **A1**, 6 (2007).

[23] I.P. Ivanov, *Phys. Rev.* **D68**, 032001 (2003).

[24] D.Yu. Ivanov, L. Szymanowski, G. Krasnikov, *JETP Lett.* **80**, 226 (2004); M. Diehl, W. Kugler, *Eur. Phys. J.* **C52**, 993 (2007).

[25] A.D. Martin, M.G. Ryskin, T. Teubner, *Phys. Rev.* **D55**, 4329 (1997).

[26] A. Levy [ZEUS Collaboration], *Acta Phys. Pol. B* **33**, 3547 (2002).

[27] D.Yu. Ivanov, R. Kirschner, *Phys. Rev.* **D58**, 114026 (1998); E.V. Kuraev, N.N. Nikolaev, B.G. Zakharov, *JETP Lett.* **68**, 696 (1998).

[28] K. Schilling, G. Wolf, *Nucl. Phys.* **B61**, 381 (1973).

[29] J. Breitweg *et al.* [ZEUS Collaborations], *Eur. Phys. J.* **C12**, 393 (2000); C. Adloff *et al.* [H1 Collaboration], *Eur. Phys. J.* **C13**, 371 (2000).

[30] C. Adloff *et al.* [H1 Collaboration], *Phys. Lett.* **B541**, 251 (2002).

[31] M. Atkinson *et al.* [Omega Photon Collaboration], *Z. Phys.* **C26**, 499 (1985); *Z. Phys.* **C30**, 531 (1986).

[32] A.D. Martin, M.G. Ryskin, T. Teubner, *Phys. Rev.* **D56**, 3007 (1997).

[33] G. Kulzinger, H.G. Dosch, H.J. Pirner, *Eur. Phys. J.* **C7**, 73 (1999).

[34] F. Caporale, I.P. Ivanov, *Phys. Lett.* **B622**, 55 (2005).

[35] F. Caporale, I.P. Ivanov, *Eur. Phys. J.* **C44**, 505 (2005); I.P. Ivanov, S. Pacetti, *Eur. Phys. J.* **C53**, 559 (2008).